



# Electrical arc contour cutting based on a compound arc breaking mechanism

Guo-Jian He<sup>1</sup> · Lin Gu<sup>1</sup> · Ying-Mou Zhu<sup>1</sup> · Ji-Peng Chen<sup>2</sup> · Wan-Sheng Zhao<sup>1</sup> · K. P. Rajurkar<sup>3</sup>

Received: 26 June 2021 / Revised: 22 October 2021 / Accepted: 17 February 2022 / Published online: 26 July 2022  
© Shanghai University and Periodicals Agency of Shanghai University and Springer-Verlag GmbH Germany, part of Springer Nature 2022

**Abstract** Electrical arc contour cutting (EACC) is a novel high-efficiency material cutting process that applies arc plasma to perform efficient and economical contour cutting of difficult-to-cut materials. Compared to conventional electrical arc machining (EAM), this process can remove the allowance of open structures and plates in bulk mode, rather than entirely in the form of debris. Compared with existing contour cutting methods, EACC possesses the advantages of high cutting efficiency and a deep cutting depth. Particularly, a compound arc breaking mechanism (CABM), which integrates hydrodynamic force and mechanical motion, has been applied to control the discharge arc column in EACC, while also strengthening the debris expelling effect in the narrow discharge gap. The CABM implementation conditions were studied, based on arc column distortion images captured by a high-speed camera and simulation results of the flow field and debris distribution. A set of machining experiments was designed and conducted to optimize the performance of the proposed process. Finally, a SiC<sub>p</sub>/Al metal matrix composite (MMC) space station workpiece was machined to verify the feasibility and efficiency of this process.

**Keywords** Electrical arc contour cutting (EACC) · Electrical arc machining (EAM) · Compound arc breaking mechanism (CABM) · SiC<sub>p</sub>/Al metal matrix composite (MMC) · High efficiency

## 1 Introduction

To guarantee their strength and reliability, many modern aerospace parts are constructed from large integrated castings or forged parts. However, this presents a challenge to machining: the majority of these parts are made of difficult-to-cut materials, such as Ni-based superalloys, titanium alloys, and metal matrix composites (MMCs). Furthermore, it is worth noting that, typically, over 80% of the material should be removed [1, 2]. However, most allowances are generally removed using point-to-point modes, such as milling, electrical discharge machining (EDM), or electrochemical machining (ECM) [3]. Converting all the unneeded material into debris takes considerable energy and time. This not only increases the processing cost, but also wastes a significant amount of energy and material.

The machining efficiency and material recycling ratio can be vastly improved through adopting an approach that first uses contour cutting to quickly remove most of the allowance and then uses a point-to-point mode to complete the processing. At present, the primary contour cutting methods include wire electrical discharge machining (WEDM), plasma cutting, abrasive waterjet cutting, and laser cutting. However, when processing the advanced materials mentioned above, the existing contour cutting methods are limited by their machining efficiency and shallow cutting depth [4, 5].

Electrical arc machining (EAM) is a promising method for machining difficult-to-cut materials with certain advantages, such as excellent material removal capabilities and

✉ Lin Gu  
lgu@sjtu.edu.cn

<sup>1</sup> State Key Laboratory of Mechanical System and Vibration, School of Mechanical Engineering, Shanghai Jiao Tong University, Shanghai 200240, People's Republic of China

<sup>2</sup> School of Mechanical and Electronic Engineering, Nanjing Forestry University, Nanjing 210037, People's Republic of China

<sup>3</sup> Center for Nontraditional Manufacturing Research, University of Nebraska-Lincoln, Lincoln, NE, USA

a low cost [6, 7]. Studies show that when machining the Inconel 718 alloy, Ti-6Al-4V, and SiC<sub>p</sub>/Al metal matrix composites with EAM, the material removal rate (MRR) is overwhelmingly high and accompanied by a limited tool wear ratio (TWR) [8–10]. This is because EAM removes material with high-energy concentrated plasma whose machining capability is independent of the material's mechanical properties, such as hardness and stiffness [11].

EAM and EDM are both electrical processing methods. EAM was first proposed in 1988 [12] to solve EDM's low-efficiency problem. In comparison with EDM, the discharge current applied in EAM can be hundreds or even thousands of amperes and results in an arc column temperature above 10<sup>4</sup> K, which can melt or even vaporize all conductive materials. Except for the significant increase in current, the pulse duration in EAM can reach milliseconds, while that in EDM is microseconds. Moreover, there is no obvious breakdown delay in the EAM voltage waveforms. The above differences lead to a huge increase in the EAM discharge energy.

However, a highly energized electrical arc is prone to localize and damage the workpiece surface [13]. Thus, effective arc control methods that drive the arc column to move on the workpiece or break down in time to prevent the formation of a stationary arc are important and necessary. In EAM, arc control methods are also known as arc breaking mechanisms. Generally, two types of arc breaking mechanisms are applied in EAM. The first is a mechanical motion arc breaking mechanism, which is induced by relative movements between the electrode and the workpiece [13]. Alternatively, the hydrodynamic arc breaking mechanism uses intensive internal or external flushing to drive the arc to stretch or move on the workpiece surface [14, 15]. Kou and Han [13] conducted a theoretical analysis of the moving electric arcs caused by relative movements, and used photos of the plasma channel to verify the motion of arcs on the workpiece surface. Meanwhile, Gu et al. [14] explored the development of the arc plasma channel under hydrodynamic forces and analyzed the crater formation mechanisms of a single arc discharge. Additionally, Zhang et al. [15] continued to study the high-velocity flushing effect in EAM applying the computational fluid dynamic (CFD) method. Their results indicated that high-velocity flushing not only disturbed the stability of the arcing but can also form a low-pressure area on the downstream side of the electrode. This induces a negative pressure suction effect, which can more efficiently evacuate melting metal from a melting pool, and results in a high MRR, as well as a thin heat-affected zone (HAZ).

A variety of EAM methods have been developed for different processing requirements, such as die-sinking EAM [16], arc milling [17], arc turning [18], and arc sweep machining [19]. However, the available EAM methods have to remove the allowance entirely as debris, rather than in

bulk mode. In this research, a novel contour cutting method, namely electrical arc contour cutting (EACC), is proposed based on the principle of EAM.

The electrodes and mechanism to achieve effective arc breaking in EACC are significantly different from existing EAM methods. EACC performs contour cutting along a pre-defined path with a long, thin rotating rod electrode. Compared with removing material in point-to-point mode, EACC can significantly improve the material removal efficiency by separating the unneeded material in bulk mode. Moreover, the high energy density of the arc enables EACC to be more effective than other currently available machining processes for contour cutting difficult-to-cut material. However, EACC has a narrow gap and a large machining depth, resulting in more severe processing conditions than other EAM methods. Therefore, it is vital to implement a more effective arc breaking strategy while machining with EACC. To solve this problem, a compound arc breaking mechanism (CABM) that combines hydrodynamic force and mechanical movement was applied. In addition, this paper investigated the arc distortion effect in the CABM, through images captured at high speed and CFD simulation, and studied the debris expelling effect through debris particle distribution simulation. Afterwards, a set of machining experiments was designed and conducted to optimize the performance of the proposed process. Finally, a SiC<sub>p</sub>/Al MMC workpiece was machined to verify the feasibility and efficiency of this process.

## 2 Principle of EACC

The composition of the EACC system is illustrated in Fig. 1. Specifically, it mainly includes a five-axis computer numerical control (CNC) machine, an electrode holder, a high-pressure flushing unit, and a high-energy power supply. The electrode holder is specially designed to integrate multiple functions, including electrode rotation, transmitting electric power to the electrode, and providing high-velocity coaxial flushing. The high-energy power supply provides discharge energy for arc machining, and can generate a current of thousands of amperes. The flushing holes are distributed evenly on the tool holder, which can provide powerful flushing to the discharging area.

Figure 2 depicts the schematic diagram of the EACC process. During the machining process, a long, thin rotating rod electrode cuts deeply into the workpiece and performs EAM with its side surface. As an arc machining process, the arc plasma in the gap should be well controlled to avoid constant arcing and short circuits. In conventional EAM, the electrode diameter is usually greater than 10 mm, and its end can be arranged with flushing holes to achieve strong internal flushing. Internal flushing directly acts on the discharge area, resulting in a better effect on the arc control and debris

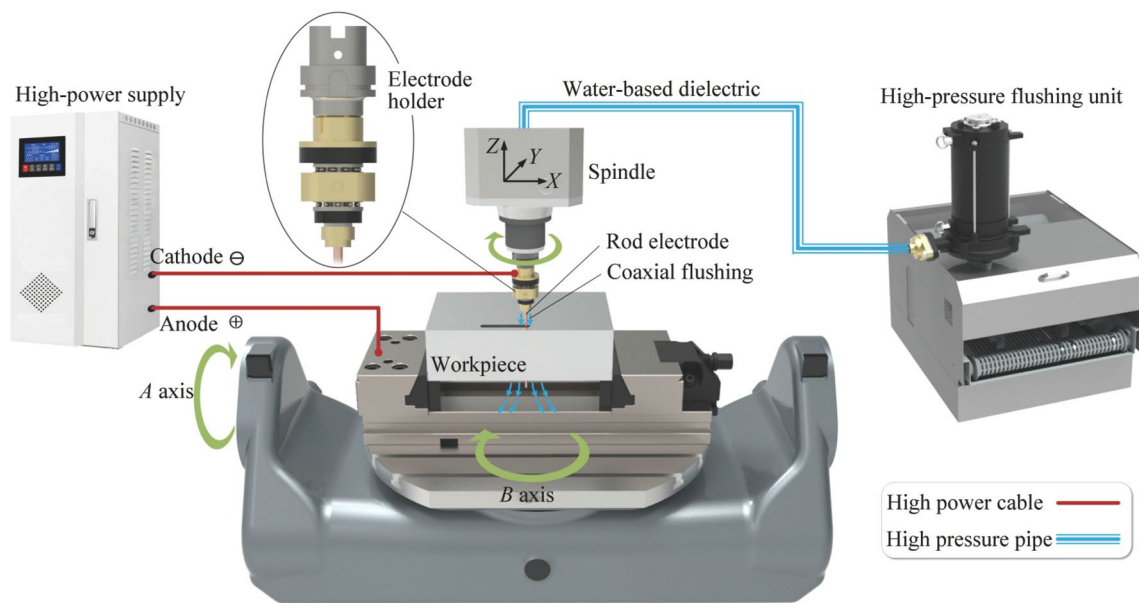


Fig. 1 Diagram of an EACC system

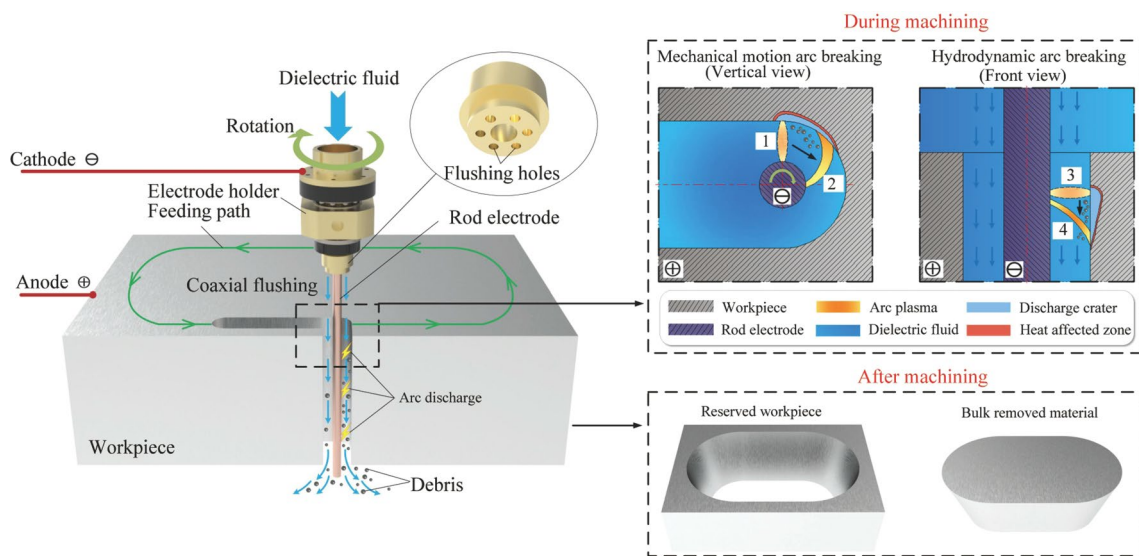


Fig. 2 Schematic diagram of EACC

expelling. Meanwhile, at the same rotation speed, a larger electrode diameter can achieve a higher relative motion speed between the electrode and workpiece, which is beneficial for realizing mechanical motion arc breaking.

On the other hand, the thin rod electrode used in EACC cannot achieve internal flushing and slows the relative motion speed. Compared with conventional EAM, the machining depth in EACC is greatly increased, which is not conducive to debris expelling. Debris particles tend to accumulate in the narrow discharge gap and cause constant arcing and short circuits. In short, owing to the small electrode

diameter and deep cutting depth, it is very difficult to achieve effective arc breaking conditions with either mechanical motion or hydrodynamic force in EACC.

Under such circumstances, a CABM that combines mechanical movement and hydrodynamic force was applied to boost the arc control capacity and promote the debris expelling effect. Specifically, as demonstrated in Fig. 2, the electrode rotates with the spindle and drives the arc column to slide on the workpiece surface (from position 1 to position 2), which directs the mechanism of mechanical motion arc breaking. Meanwhile, coaxial flushing holes on the tool

holder provide a powerful flushing toward the discharge gap, which performs the hydrodynamic arc breaking mechanism. In this process, it drives the arc plasma column along the flushing direction (from position 3 to position 4) and expels the melting metal out of the discharge gap, as well as cooling the arced area. Ultimately, the CABM is accomplished by hybridizing rapid electrode rotation and high-velocity coaxial water flushing in the EACC. Based on this, a surface profile can be achieved on the workpiece by directing the rod electrode along the predefined trajectory, and excessive material allowance can be removed as a whole.

### 3 Implementation of the compound arc breaking mechanism

#### 3.1 Mechanical motion arc breaking

To investigate the influence of the mechanical motion on arc control, a high-speed camera was utilized to capture images of the arc plasma in a single arc discharge, when the workpiece and electrode moved at different speeds. Figure 3 shows that when there is no relative motion between the electrode and workpiece, the arc plasma column is

symmetrically distributed in a bell shape, which means that the arc plasma localizes on the workpiece surface. As the relative motion speed increases, the arc plasma column distorts gradually and shifts in the direction of the workpiece movement.

Figure 3 reveals that when the relative motion speed reaches 1 m/s, the arc plasma begins to move along the workpiece surface, which demonstrates that the arc is effectively controlled. Consequently, a relative motion speed of 1 m/s can be regarded as the critical condition of the mechanical motion arc breaking mechanism. Since the maximum rotating speed of the tool holder is approximately 3 000 r/min, the electrode diameter should be greater than 6 mm to reach a relative speed of 1 m/s at the workpiece interface.

#### 3.2 Hydrodynamic arc breaking

As shown in Fig. 4, previous research in our lab revealed that as the flushing velocity increased, the distortion of the arc column increased accordingly. The arc/workpiece interface travelled more than 5 mm along the flushing direction when the velocity was 7 m/s [14]. In contrast, no obvious arc plasma deformation was identified when the flushing velocity was lower than 7 m/s. Consequently, a flushing velocity

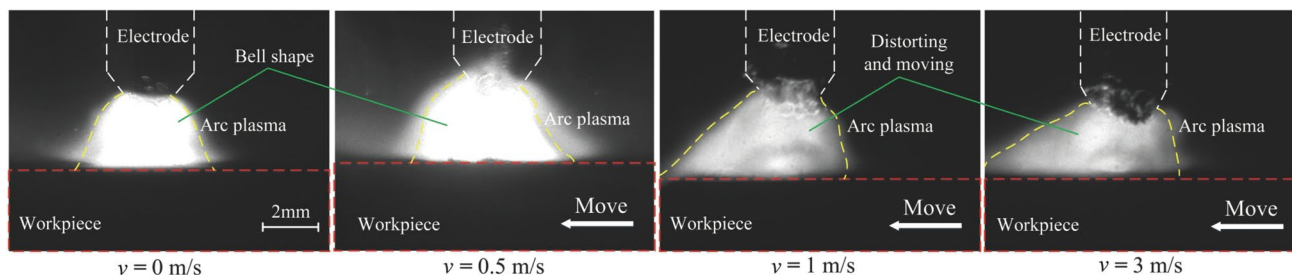


**Fig. 3** Arc plasma distortion under mechanical motion arc breaking mechanism

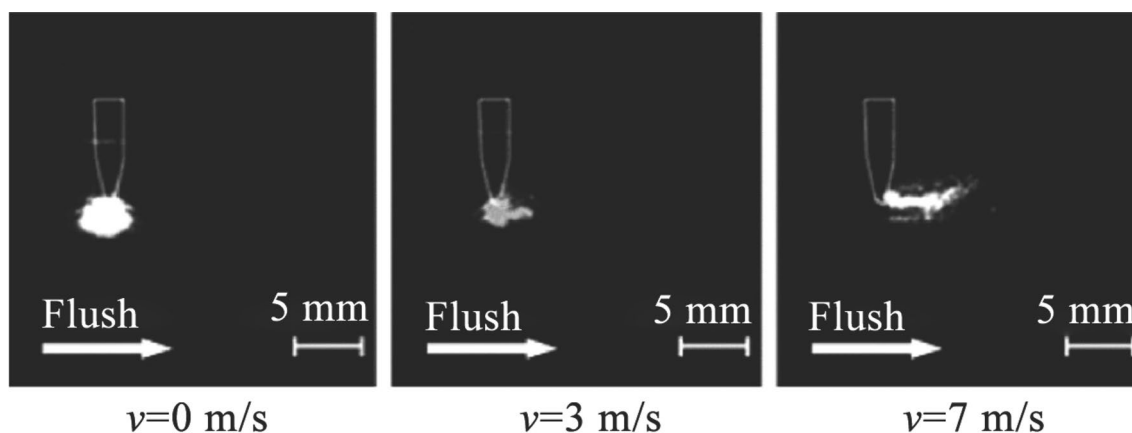


**Fig. 4** Arc plasma distortion under hydrodynamic arc breaking mechanism [14]

of 7 m/s can be regarded as the critical condition to realize the hydrodynamic arc breaking mechanism. In EACC, the flushing flow field distribution in the discharge gap is mainly affected by the cutting depth. To further determine the effective range of the cutting depth and explore the positive effect of CABM on debris expelling in narrow discharge gaps, the flow field and debris particle distribution were simulated, as described in the following section.

## 4 Simulation of the flow field and debris distribution

### 4.1 Simulation conditions for EACC

During EACC machining, six flushing holes are evenly distributed around the electrode to perform coaxial flushing. The flow field simulation analysis only considers the flushing area, including the rotating electrode and static workpiece. Figure 5 shows a schematic diagram of the EACC flushing condition and the simplified computational domain. According to the machining conditions, the coaxial flushing between the nozzle and the upper surface of the workpiece is regarded as a rotating fluid region, driven by the rotation of the coaxial nozzle. A continuity interface is added between the upper coaxial flushing rotation region and the flushing fluid in the gap. The workpiece material in the simulation is set to 20% (volume fraction) SiC<sub>p</sub>/Al.

To meet the critical condition for realizing the mechanical motion arc breaking mechanism, the diameter of the electrode is set to 6 mm, and the rotation speed is set to 3 000 r/min in the geometric model. Meanwhile, the length of the

rotating flushing fluid column is set to 15 mm. The flushing fluid thickness between the electrode and the workpiece is set to 0.5 mm, which is the same as the discharge gap. Moreover, the fluid thicknesses away from the machining area are 2 mm, the same as the flushing hole diameter. The volume between the upper coaxial flushing rotating region and the gap bottom is set as a buffer region that contains the rotation domain interface. The buffer region means that when the flushing fluid reaches the workpiece surface, only part of it can rush into the discharge gap, while the remainder flows past. Four cutting depths, 20 mm, 30 mm, 40 mm, and 50 mm, were selected to assess the influence of the flushing depth on the flow field and debris particle distribution in the gap.

In the simulation, the water fluid inlet is the top surface of the nozzle, and the inlet reference pressure is 1.0 MPa. The flushing fluid outlet area is derived from the area surrounding the discharge gap, and its reference pressure is set to zero. It should be noted that the discharge crater formed in arc machining is greater than that in ordinary discharge machining, and it results in a coarser surface, which disturbs the flushing effect in the narrow gap. Because of this, the roughness of the machined surface is set to 40 μm, which is based on experimental results [20, 21].

According to the calculated Reynolds number of the simulation, the flushing fluid is in a turbulent state, and the standard *k-ε* model was chosen to calculate the flow field in the gap. In this research, the turbulence module and the rotating machinery module in COMSOL Multiphysics software were applied. Additionally, a uniform pair between the coaxial flushing rotation domain and the flushing fluid in the discharge gap was defined. The Frozen Rotor study was

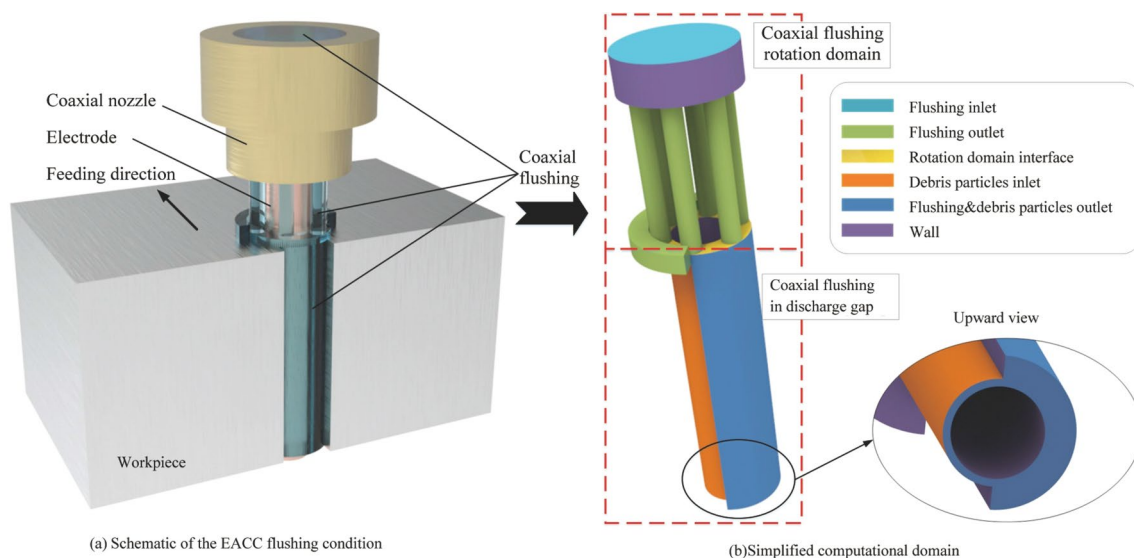


**Fig. 5** Simulation model of the flow field and debris distribution

used to simulate the velocity and pressure fields in rotating machinery and calculate the initial conditions for time-dependent simulations of flow fields in rotating machinery.

During the EACC process, many debris particles are generated periodically in the discharge area. Excessive particles in the gap result in unstable discharging or even short circuiting. Hence, the particles were traced in the flow field, based on the flow field simulation results. The particle tracing simulation was implemented under a peak current of 500 A, a pulse duration of 5 ms, and a pulse interval of 3 ms. According to previous experimental results, when the peak current is 500 A, the average particle diameter is around 100  $\mu\text{m}$ . Approximately 400 particles are randomly generated on the surface when the pulse duration  $T_{\text{on}}$  is 5 ms and the pulse interval  $T_{\text{off}}$  is 3 ms. The inlet and outlet of the debris particles are also marked in Fig. 5.

## 4.2 Results of the flow field simulation

Figure 6 shows the simulation results for the flow field at different cutting depths. All results demonstrate that the velocity of the coaxial flushing rotating domain is greater than 25 m/s. However, owing to the limitations of the narrow gap and deep cutting depth in EACC, the flushing velocity decreases rapidly in the discharge gap, and its maximum is less than 15 m/s. In addition, as the cutting depth increases, the velocity of the dielectric fluid decreases significantly. The results revealed that the relatively rough surface and narrow machining gap retarded the flushing and thereby weakened the hydrodynamic arc breaking effect in the deep area.

To analyze the flushing velocity in the discharge gap under different cutting depths, axial sectional and bottom

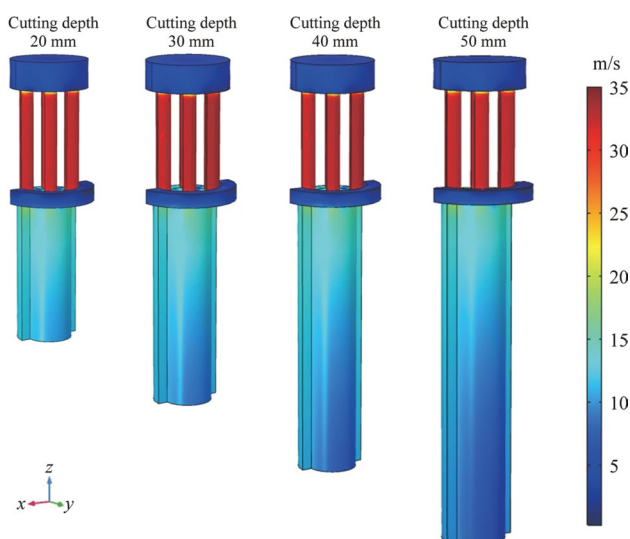


**Fig. 6** Results of the flow field simulation for different cutting depths

views of the flushing velocity distribution are compared, as shown in Fig. 7. In each axial sectional view, the right column represents the inflow to the discharge gap, and the left column represents the outflow around the electrode. It should be noted that the flushing velocity decreases significantly as the cutting depth increases. The maximum flushing velocity is approximately 15 m/s at the gap entrance, and then decreases to 7.2 m/s when the cutting depth is 40 mm. This indicates that the rough surface of the discharge area in the narrow discharge gap impedes the flushing effect, which leads to poor discharging conditions. When the cutting depth is 50 mm, the flushing velocity in parts of the gap is less than 7 m/s, and the minimum velocity is 5.9 m/s. Because the critical flushing velocity to realize the hydrodynamic arc breaking mechanism is 7 m/s, the cutting depth should not exceed 40 mm in EACC. When cutting a thick workpiece, layered cutting with a single cut depth of less than 40 mm is considered to be more effective.

## 4.3 Results of debris distribution simulation

When the cutting depth was 20 mm, the debris particle distribution in an entire pulse period was simulated, as shown in Fig. 8. During  $T_{\text{on}}$ , the concentration of the generated particles did not substantially increase because intensive flushing effectively expelled the generated debris out of the gap. Furthermore, the debris concentration decreased rapidly in  $T_{\text{off}}$  because no fresh debris particles were generated. At the 7 ms time point, the number of debris particles left in the gap was 15, and no debris particles were left at 8 ms. This means that the EACC process can be performed continuously and normally under this condition.

Because the number of residual particles at the end of each discharge pulse has an important effect on the discharge state, the distribution of the debris particles during the pulse interval is brought into focus. Figure 9 illustrates the debris distribution in pulse intervals at different cutting depths. As shown, the concentration of the remaining debris particles increases with the increasing cutting depth. For a 30 mm cutting depth, the number of remaining debris particles is approximately 12 at 8 ms, which is slightly larger than that at the 20 mm cutting depth. As the cutting depth is increased to 40 mm, the debris particle concentration further increases to 27 at 8 ms. This means that a longer pulse interval is necessary when the cutting depth increases. Furthermore, when the cutting depth is 50 mm, it is impossible to achieve an effective CABM, and numerous debris particles remain in the gap at the end of the discharge. An optimization experiment was conducted to identify and optimize the cutting depth under different conditions.

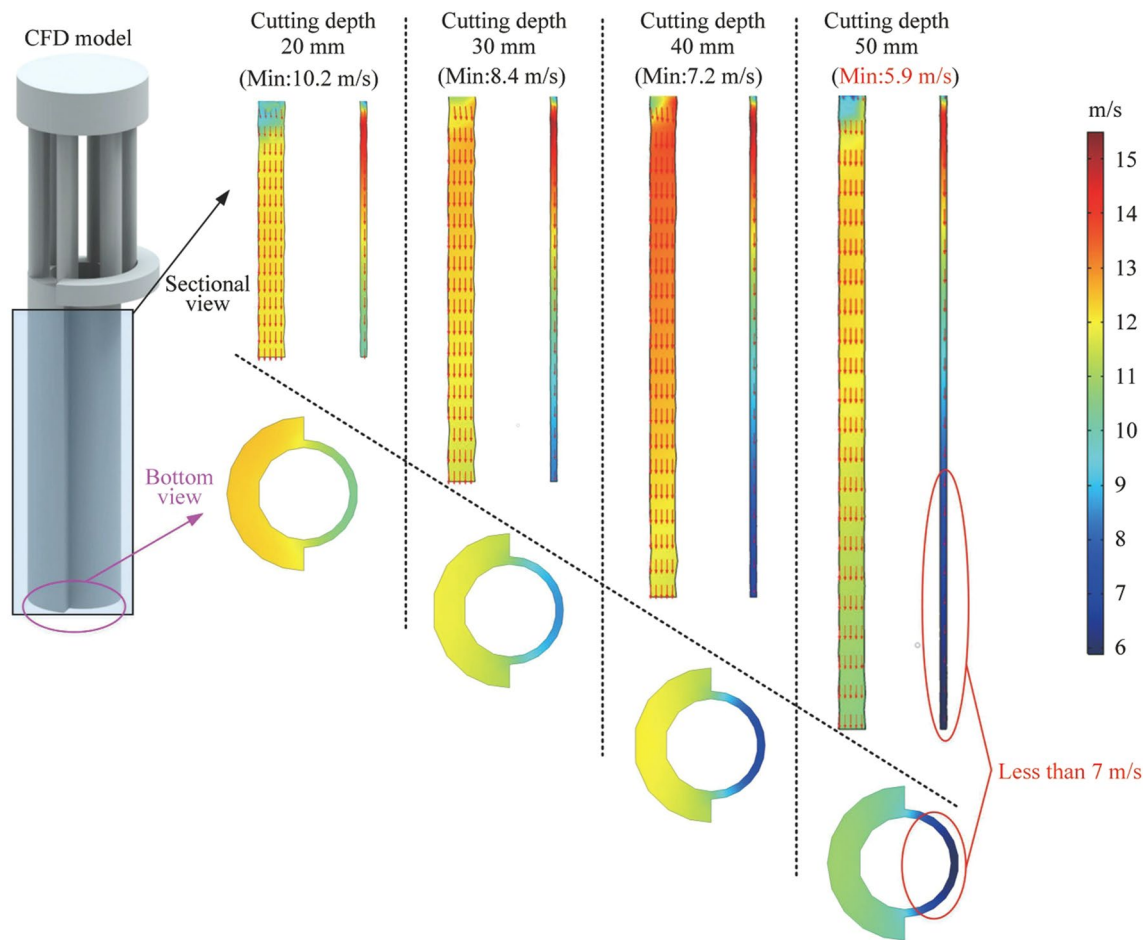


Fig. 7 Sectional and bottom views of the flushing velocity under different cutting depths

## 5 Experimental setup and design

### 5.1 Experimental setup

Parameter optimization experiments were conducted with a self-renovated BEAM CNC machine tool. A high-power supply with a maximum current of 1 500 A was connected to the electrode and workpiece to provide discharge energy. During the machining process, the CABM was applied to control the discharge arc and expel debris from the narrow discharge gap. To achieve this mechanism, a special electrode holder was designed to perform electrode rotation and high-velocity coaxial flushing, which can be observed in Fig. 10.

### 5.2 Experimental design

The influence of significant factors on the machining performance was further studied. The peak current, pulse duration, and cutting depth were chosen, based on previously conducted fractional factorial experiments.

Particularly, the experiments mainly focused on the cutting efficiency of the EACC method. The cutting efficiency is represented by the cutting area efficiency (CAE) and the MRR. The CAE represents the ratio of the cut surface area to the machining time, while the MRR refers to the volume of material removed per minute.

The workpiece material was 20% (volume fraction)  $\text{SiC}_p/\text{Al}$ , a difficult-to-cut metal matrix composite. The cylindrical electrode was a tungsten rod with 6 mm diameter and 200 mm in length. The electrode and the workpiece were connected to the negative and positive poles of the power supply, respectively. Meanwhile, the open voltage of the power supply was set to 90 V, and  $T_{\text{off}}$  was fixed at 3 ms. The dielectric fluid used in the experiments was water, the same as that in the simulation. According to the flow field simulation results at different cutting depths in the above section, a cutting depth greater than 40 mm is not conducive to CABM, so depths of 10, 20, 30 and 40 mm were chosen for optimization. Other parameters are listed in Table 1.

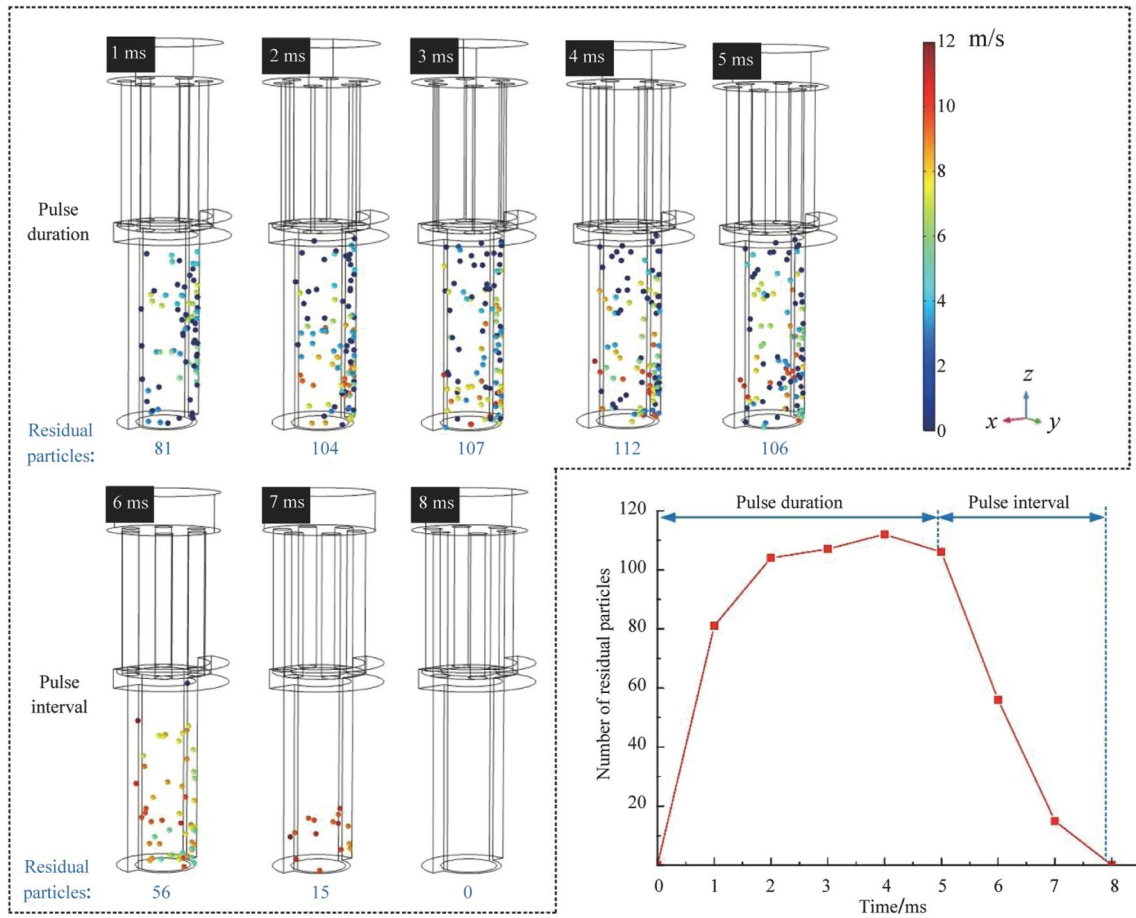


**Fig. 8** Debris particle distributions at 20 mm cutting depth

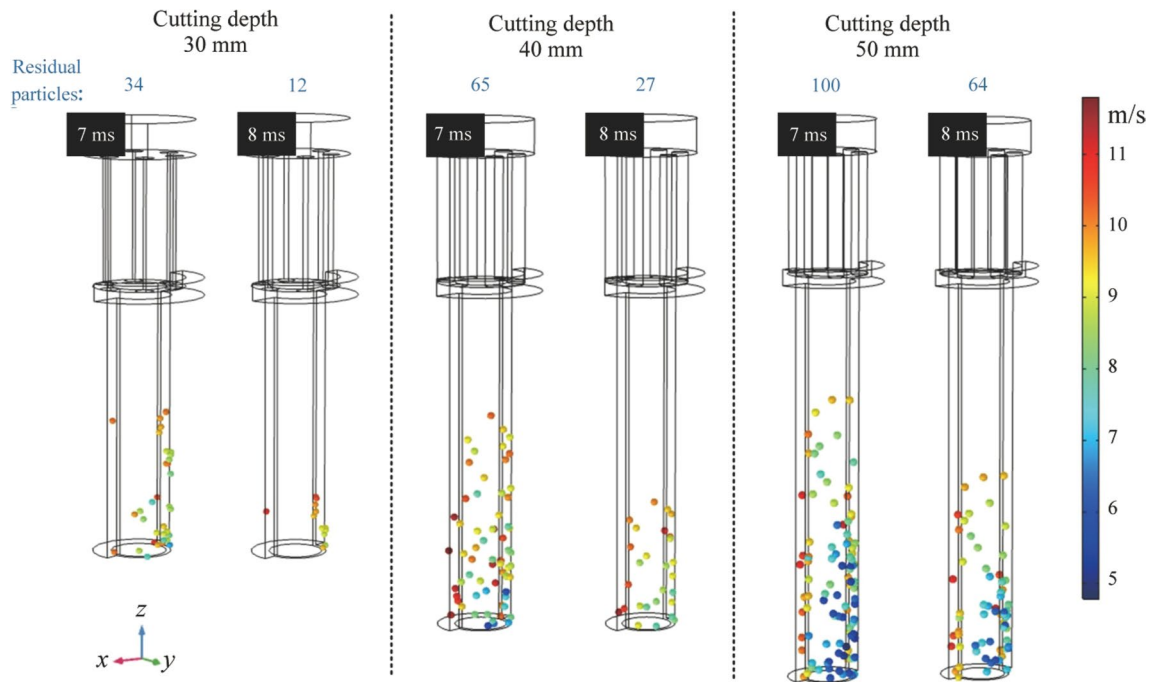


**Fig. 9** Debris particle distributions for different cutting depths



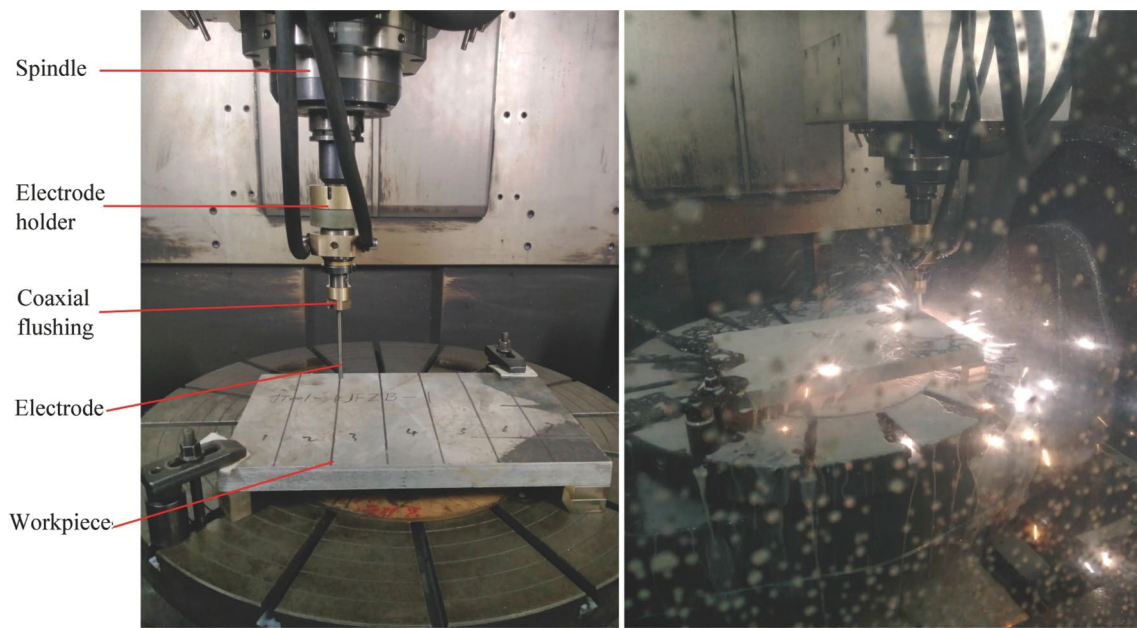


Fig. 10 Machining equipment and process

Table 1 Experiment design and parameter values (spindle speed 3 000 r/min, flushing pressure 1 MPa, open voltage 90 V, pulse interval 3 ms)

Experiment Sets	Parameter values	
	Variables	Fixed parameters
Set 1	$I_p/A$ : 100, 200, 300, 400, 500	$T_{on}$ : 5 ms/Depth: 20 mm
Set 2	$T_{on}/ms$ : 1, 3, 5, 7, 9	$I_p$ : 300 A/Depth: 20 mm
Set 3	Depth/mm: 10, 20, 30, 40	$I_p$ : 500 A/ $T_{on}$ : 5 ms

## 6 Experimental results and analysis

### 6.1 Discharge current experimental results

As shown in Fig. 11, both the CAE and the MRR increased with the increasing current. When the discharge current was 100 A, the CAE was 160 mm<sup>2</sup>/min, and the MRR was approximately 1 150 mm<sup>3</sup>/min. As the discharge current increased to 500 A, the CAE reached 900 mm<sup>2</sup>/min. To date, the maximum WEDM efficiency of SiC<sub>p</sub>/Al composites has been reported to be only approximately 90 mm<sup>2</sup>/min [4]. Based on such results, it can be said that the EACC efficiency can reach ten times that of WEDM. When the discharge current was 500 A, the maximum

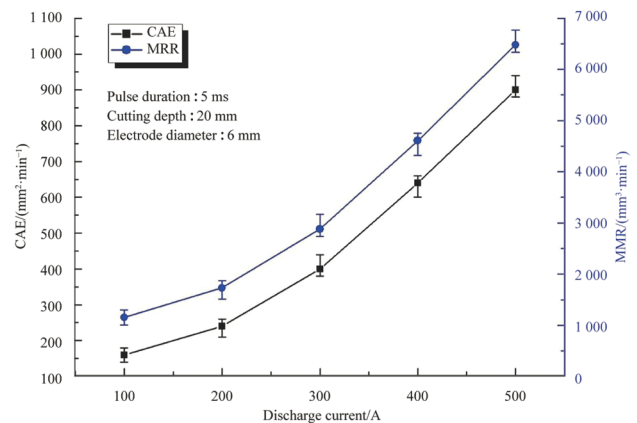
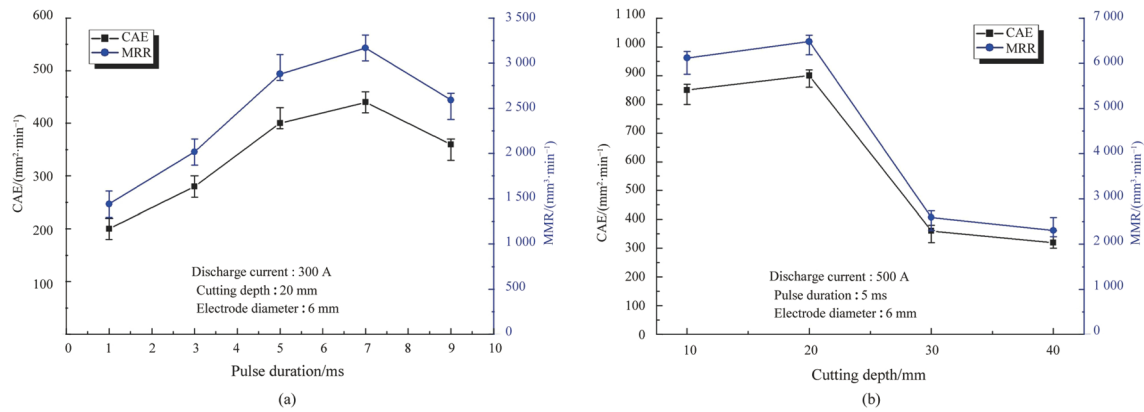


Fig. 11 Experimental results for different discharge current conditions

MRR of the EACC was 6 500 mm<sup>3</sup>/min, which was similar to that of EAM [9, 21].

### 6.2 Pulse duration experimental results

Figure 12a shows the CAE and the MRR results for different pulse duration conditions. At first, both the CAE and the MRR increase as the pulse duration increases, and when the pulse duration exceeds a certain value, they both decrease. The optimal pulse duration is approximately from 5 ms to 7 ms, under other specific experimental conditions. During the discharging process, a rise in the pulse duration means an increase in the energy supply, resulting in a higher CAE



**Fig. 12** Experimental results for different **a** pulse duration conditions and **b** cutting depths

and MRR. However, because the pulse interval was set to 3 ms in this experiment, an excessively long pulse duration with insufficient pulse intervals can lead to insufficient arc breaking and short circuits, which reduces the machining efficiency. Based on the pulse duration experimental results, the optimized pulse duration is approximately from 5 ms to 7 ms under the current experimental conditions.

### 6.3 Cutting depth experimental results

Figure 12b depicts that the CAE and the MRR increase slightly as the cutting depth increases at first, but decrease as it reaches a certain value. A reasonable explanation for this is that the increased cutting depth decreases the cutting feed rate during the EACC process. The theoretical CAE is calculated by taking the product of the cutting depth and the cutting feed rate; thus, it can be inferred that there is an optimal value between the cutting depth and the cutting feed rate.

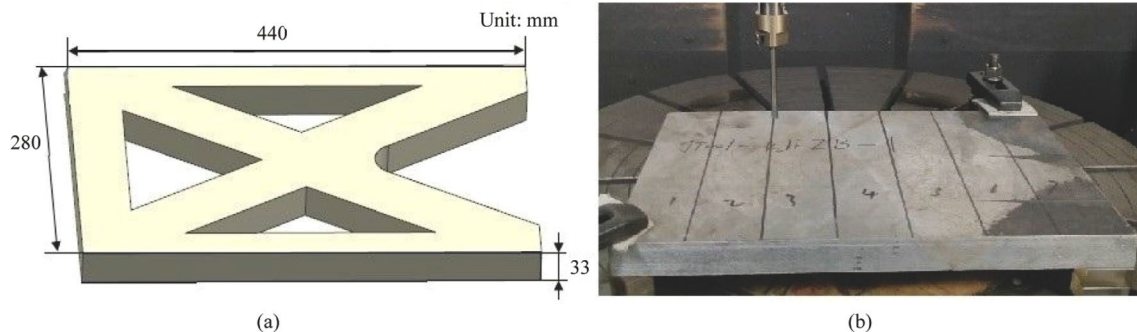
When the cutting depth is 20 mm, the CAE reaches the maximum, although the feed rate decreases slightly. However, when the cutting depth continually increases, the machining state worsens, and the feed rate significantly

decreases. The main reason is attributed to the flushing flow, which barely reaches the deepest area of the discharge gap, resulting in frequent short circuits and gathering debris. This indicates that high-velocity flushing is particularly important during the EACC process. Notably, the experimental results for cutting depths are consistent with the simulation results of debris particle distribution.

According to the results of the study, the optimized cutting layer depth is about 15–25 mm when the discharge current is around 500 A and the discharge duration is approximately 5 ms. When cutting a thick workpiece, layered cutting is recommended, rather than cutting the entire thickness in one continuous feed.

## 7 Sample machining

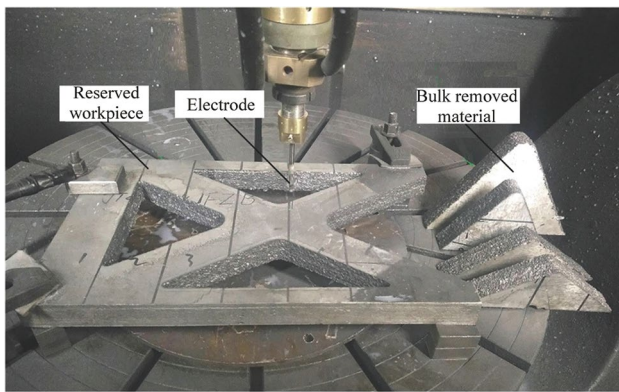
Based on the above experimental results, a 20% (volume fraction) SiC<sub>p</sub>/Al composite material solar panel supporter was roughly machined with EACC. As illustrated in Fig. 13, four triangles (approximately 40% of the total volume) are needed to be removed from a rectangular plate. Because the plate is 33 mm thick and contains many nonconductive SiC



**Fig. 13** Structure of the SiC<sub>p</sub>/Al part **a** 3D model, **b** SiC<sub>p</sub>/Al plate

particles, the wire frequently broke when applying WEDM to remove the triangles from the plate. The highest optimized CAE of WEDM is approximately  $90 \text{ mm}^2/\text{min}$ . Here, EACC was applied to remove the triangles. The thicknesses of the first layer and the second layer were 17 mm and 16 mm, respectively. The electrode diameter was 6 mm, and the discharge current was 600 A with a 5 ms pulse duration. The other conditions were the same as those in the previous experiments.

Figure 14 shows the machined workpiece and removed material. Two hours were spent on the rough machining, which was considerably shorter than that in cutting with WEDM. The average feed rate was 35 mm/min, and the average CAE of the EACC was approximately  $550 \text{ mm}^2/\text{min}$ , which was over six times that of WEDM. In addition, because the electrode material was tungsten, the electrode wear rate was very limited, and a 6 mm diameter electrode was sufficient to cut over a 400 mm length trajectory.



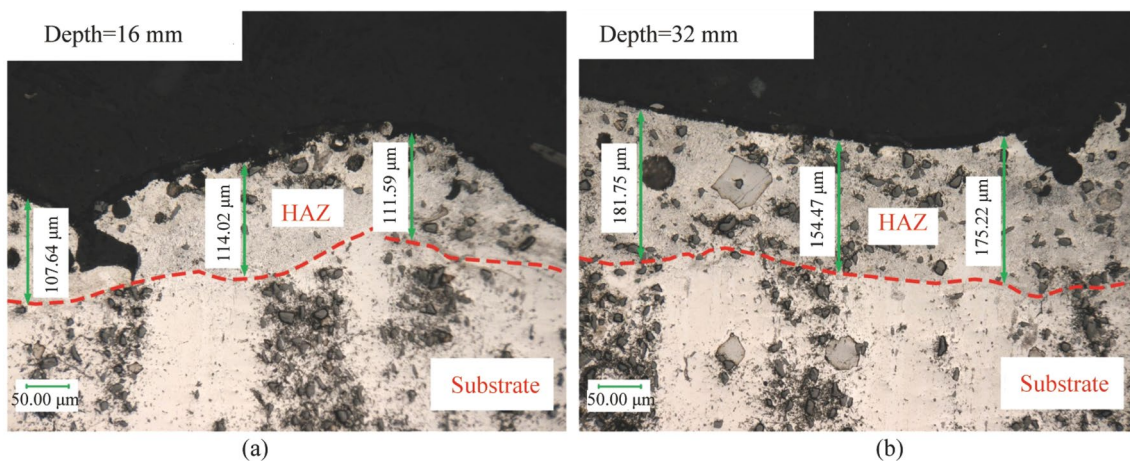
**Fig. 14** Rough machined workpiece

Figure 15 shows metallographic photographs of workpiece cross sections at depths of 16 mm and 17 mm, acquired after machining. These indicate that there is an obvious HAZ on the surface of the workpiece after EACC, and as the cutting depth increases, the thickness of the HAZ also increases. Although EACC causes the appearance of the HAZ, the maximum thickness of the HAZ is less than 200  $\mu\text{m}$ , which can be removed by the subsequent finishing process without a negative effect on the final parts. Therefore, the results of the sample machining prove that EACC is a feasible and efficient method for processing difficult-to-cut materials.

## 8 Conclusions

A highly efficient electrical arc contour cutting process with a compound arc breaking mechanism was introduced and explored in this paper. The machining parameters were optimized, based on results from previous studies and a current set of experiments. A sample part was machined to confirm the feasibility of the process. Based on the simulations and experiments, the following conclusions were drawn.

- (i) Electrical arcs can be applied to perform highly efficient contour cutting by compound arc breaking mechanism.
- (ii) A compound arc breaking mechanism can significantly promote the arc breaking and debris evacuation effects, and an optimized electrode diameter and cutting depth can be obtained for the given flushing and electrical conditions.



**Fig. 15** Metallographic photographs of workpieces at different depths

- (iii) When cutting a SiC<sub>p</sub>/Al MMC, the maximum efficiency of EACC can be ten times that of WEDM, and even greater than that of electrical arc milling.
- (iv) Like other EAM methods, the surface of the workpiece after EACC is rough and there is a non-negligible HAZ. A subsequent finishing process, such as CNC milling, grinding, or ECM, should be conducted to eliminate these negative effects.

**Acknowledgments** The authors acknowledge the National Science Foundation of China (Grants Nos. 51235007 and 51575351) and the State Key Laboratory of Mechanical System and Vibration of China (Grant No. MSV201305) for their financial support of this research.

## References

1. Klocke F, Schmitt R, Zeis M (2015) Technological and economical assessment of alternative process chains for blisk manufacture. *Proc CIRP* 35:67–72
2. Bergs T, Grünebaum T, Fricke K et al (2021) Life cycle assessment for milling of Ti- and Ni-based alloy aero engine components. *Proc CIRP* 98:625–630
3. Klocke F, Klink A, Veselovac D et al (2014) Turbomachinery component manufacture by application of electrochemical, electro-physical and photonic processes. *CIRP Ann Manuf Technol* 63(2):703–726
4. Ma B, Zhu Y, Jin X (2011) Wire electro discharge machining of Al/SiC metal matrix composite. *Appl Mech Mater* 121/126:564–567
5. Krajcarz D (2014) Comparison metal water jet cutting with laser and plasma cutting. *Proc Eng* 69:838–843
6. Zhao W, Gu L, Xu H et al (2013) A novel high efficiency electrical erosion process-blasting erosion arc machining. *Proc CIRP* 6:622–626
7. Wang F, Liu Y, Tang Z et al (2014) Ultra-high-speed combined machining of electrical discharge machining and arc machining. *Proc Inst Mech Eng B J Eng Manuf* 228(5):663–672
8. Wang F, Liu Y, Shen Y et al (2013) Machining performance of Inconel 718 using high current density electrical discharge milling. *Mater Manuf Process* 28:1147–1152
9. Gu L, Chen J, Xu H et al (2016) Blasting erosion arc machining of 20 vol.% SiC/Al metal matrix composites. *Int J Adv Manuf Technol* 87(9):2775–2784
10. Shen Y, Liu Y, Sun W et al (2015) High-speed dry compound machining of Ti6Al4V. *J Mater Process Technol* 224:200–207
11. Zhang R, Zhang Y, Liu Y et al (2017) Energy distribution and material removal of electric arc machining (EAM). *J Mater Process Technol* 242:110–116
12. Meshcheriakov G, Nosulenko V, Meshcheriakov N et al (1988) Physical and technological control of arc dimensional machining. *CIRP Ann Manuf Technol* 37:209–212
13. Kou Z, Han F (2018) Machining characteristics and removal mechanisms of moving electric arcs in high-speed EDM milling. *J Manuf Process* 189:78–87
14. Gu L, Zhang F, Zhao W et al (2016) Investigation of hydrodynamic arc breaking mechanism in blasting erosion arc machining. *CIRP Ann Manuf Technol* 65(1):233–236
15. Zhang F, Gu L, Chen J et al (2016) Observation and modeling research of high-velocity flushing effect on the performance of BEAM. *Int J Adv Manuf Technol* 86(1):935–942
16. Wang C, Cheng J, Gu L et al (2016) Blasting erosion arc machining of turbine blisk flow channel with laminated electrode. *Proc CIRP* 42:317–321
17. Chen J, Gu L, Xu H et al (2016) Study on blasting erosion arc machining of Ti-6Al-4V alloy. *Int J Adv Manuf Technol* 85:9–12
18. Liu H, Zhou J, Yu Q (2014) Analysis of mechanical quality of Nickel-base superalloy machined by short electric arc. *Asian J Chem* 26(17):5469–5472
19. Farhadi A, Gu L, Zhao W et al (2020) Tool path optimization based on wear prediction in electric arc sweep machining. *J Manuf Process* 54:328–336
20. Zhu Y, Chen J, Xu H et al (2016) Research on the surface quality of the blasting erosion arc machined stainless steel. *Proc CIRP* 42:252–256
21. Chen J, Gu L, Liu X et al (2018) Combined machining of SiC/Al composites based on blasting erosion arc machining and CNC milling. *Int J Adv Manuf Technol* 96:111–121



**Guo-Jian He** is a Ph.D. candidate at the State Key Laboratory of Mechanical System and Vibration, School of Mechanical Engineering, Shanghai Jiao Tong University, China. His research interests include the technical and equipment of electrical arc machining (EAM) and micro electrical discharge machining (Micro-EDM).



**Lin Gu** received his Ph.D. degree in Engineering from Harbin Institute of Technology. He is currently an associate professor in the State Key Laboratory of Mechanical System and Vibration, School of Mechanical Engineering, Shanghai Jiao Tong University, China. His research interests include advanced manufacturing technology for difficult-to-cut materials, such as EDM, arc discharge machining, and compound machining.



**Ying-Mou Zhu** is a Ph.D. candidate at the State Key Laboratory of Mechanical System and Vibration, School of Mechanical Engineering, Shanghai Jiao Tong University, China. His research interests include EDM, WEDM and Blasting erosion arc machining (BEAM).



**Ji-Peng Chen** received his Ph.D. degree from the State Key Laboratory of Mechanical System and Vibration, School of Mechanical Engineering, Shanghai Jiao Tong University, China. He is currently an assistant professor at School of Mechanical and Electronic Engineering, Nanjing Forestry University, China, and a visiting scholar at Polytechnic University of Milan, Italy. His research interests include advanced manufacturing technology.



**K. P. Rajurkar** is a distinguished professor at University of Nebraska-Lincoln, Lincoln, USA. He received his Ph.D. degree from Michigan Technological University. His research interests include modeling and analysis of manufacturing processes, systems sensing and control of traditional and nontraditional macro, micro and nano manufacturing processes.



**Wan-Sheng Zhao** is a professor at Shanghai Jiao Tong University, Shanghai, China. He received his Ph.D. degree in Engineering from Harbin Institute of Technology. His research interests include advanced manufacturing technologies, such as electrical discharge machining, arc discharge machining.